Electro-optical characterizations to study minority carrier transport in Ga-free InAs/InAsSb T2SL XBn midwave infrared photodetector

Vignesh Arounassalame, Maxime Bouschet, Rodolphe Alchaar, A. Ramiandrasoa, Sylvie Bernhardt, Clara Bataillon, Jean-Philippe Perez, Philippe Christol, Isabelle Ribet-Mohamed

Electro-optical characterizations to study minority carrier transport in Ga-free InAs/InAsSb T2SL XBn midwave infrared photodetector

V. Arounassalame[a], M. Bouschet[b], R. Alchaar[b], A.Ramiandrasoa[a], S.Bernhardt[a], C. Bataillon[b], J-P. Perez[b], P.Christol[b], and I.Ribet-Mohamed[a]

[a]ONERA, Chemin de la Hunière, 91761 Palaiseau, France
[b]IES, Univ.Montpellier, CNRS, F-34000 Montpellier, France

ABSTRACT

In this communication, we report on electrical and electro-optical characterizations of InAs/InAsSb Type-II superlattice (T2SL) MWIR photodetector, showing a cut-off wavelength at 5 µm. The device, made of a barrier structure in XBn configuration, was grown by molecular beam epitaxy (MBE) on GaSb substrate. At 150K, dark current measurements shows a device in the Shockley-Read-Hall (SRH) regime but with an absolute value comparable to the state-of-the-art. A quantum efficiency of 50% at the wavelength of 3 µm for a 3 µm thick absorption layer is found in simple pass configuration and front-side illumination. Combined with lifetime measurements performed on dedicated samples through time resolved photoluminescence (TRPL) technique, mobility is extracted from these measurements by using a theoretical calculation of the quantum efficiency thanks to Hovel's equations. Such an approach helps us to better understand the hole minority carrier transport in Ga-free T2SL MWIR XBn detector and therefore to improve its performance.

Keywords: InAs/InAsSb superlattice, XBn, carrier transport, lifetime, infrared detector, bariode, diffusion length, mobility, Quantum efficiency, dark current, midwave infrared

1. INTRODUCTION

In the past decade, Type-II superlattice (T2SL) infrared (IR) photodetectors based on a barrier design (called XBn) have seen significant improvements of their performance. Several years ago, it was observed that Ga-free InAs/InAsSb T2SL's carrier lifetime was significantly longer[1] than Ga-containing InAs/GaSb's one. This finding triggered intensive developments[2–7] for IR detectors based on Ga-free T2SL. However, such T2SL system has also its own challenges which need to be investigated, in particular concerning the transport of minority carriers and its relation to design and growth parameters. Transport through the superlattice (SL) in the growth direction is a key element in the design of IR detectors, since the carrier conduction in this direction determines the collection efficiency in the device. Different studies have been realized so far using different theoretical and experimental techniques.[8–10]

In this paper, we report the extraction of different transport parameters of an InAs/InAsSb T2SL XBn detector. The XBn device design consists of a unipolar conduction band barrier layer (BL) inserted between n-type absorber and contact layers (AL and CL respectively). The BL with a large bandgap material blocks the flow of majority carriers without impeding the transport of minority carriers (holes here). Dark current measurements show that the device is in the Shockley-Read-Hall (SRH) regime but with an absolute value comparable to the state-of-the-art. A quantum efficiency of 50% at the wavelength of 3 µm for a 3 µm thick absorption layer is found in simple pass configuration and front-side illumination. Combined with lifetime measurements performed on dedicated samples through time resolved photoluminescence (TRPL) technique, mobility is extracted from these measurements by using a theoretical calculation of the quantum efficiency thanks to Hovel's equations.[11] The mobility values show that miniband transport conduction does not occur and hopping transport is more likely to be the mechanism used by the carriers.

2. EXPERIMENTAL SET-UP

2.1 MATERIAL

In this work, we studied a mid-wave infrared (MWIR) T2SL heterostructures as illustrated in Fig.1. Figure.1.a, shows the stacking of the MWIR Ga-free T2SL barrier photodetector. The T2SL detector studied in this work was epitaxially grown on 2-inch n-type (Te-doped) GaSb (100) substrate by molecular beam epitaxy (MBE) using a 412 RIBER Machine. From bottom to top, the XBn structure consists of a 400 nm Te-doped (n-type) GaSb buffer layer, which is followed by a 100 nm thick n-type doped InAs/$InAs_{0.65}Sb_{0.35}$ T2SL and by non-intentionally doped (nid) 3 µm thick AL (536 periods) made of the same T2SL structure. A BL is then made from 100 nm nid $AlAs_{0.09}Sb_{0.91}$ and finally, the CL of the structure is composed of an 80 nm thick nid T2SL. The AL, CL, and BL are undoped, and the residual doping is expected to be n-type for the two first layers and p-type for the third one, at 3.10^{15} cm^{-3} and 2.10^{16} cm^{-3}, respectively.[7] More details on the structure can be found in.[12]

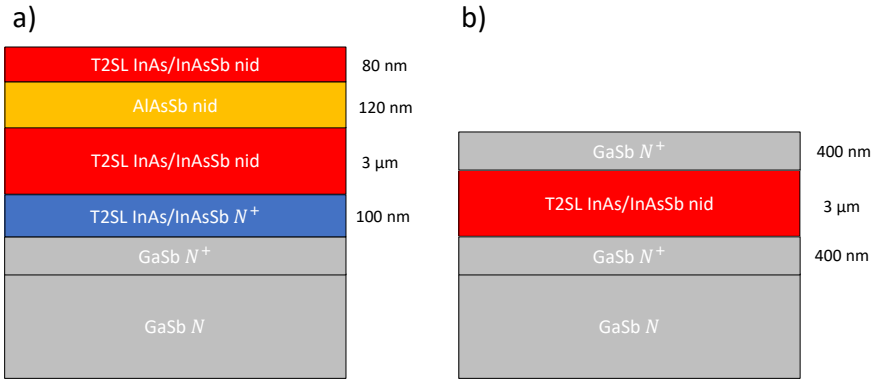

Figure 1: Schematic layout of the epilayers stacking for the structures studied. a) the complete structure for dark current and quantum efficiency studies, b) the dedicated sample for lifetime and absorption studies.

From epitaxial T2SL structures, circular mesa photodetectors with diameters ranging from 60 µm to 310 µm were fabricated using standard photolithography techniques, they were etched to the bottom of the absorber. Mesa photodetectors were realized by isotropic wet etching using a citric acid solution. No active passivation process has been applied on mesa sidewalls. A polymerized photoresist was spun after the wet etching to protect the mesa surface from ambient air. A metal coating was applied on the n-GaSb substrate and the n-type T2SL cap layer. Such devices were used to perform dark current voltage photoresponse measurements and time resolved photoluminescence (TRPL). In addition to the device samples, dedicated T2SL structures were grown to study material properties (Fig. 1.b). Such samples, consisting of a 3 μm thick InAs/InAsSb T2SL layers sandwiched between two GaSb layers providing carrier barrier confinement, were used to investigate absorption measurements.

2.2 EXPERIMENTAL BENCH

To extract material properties as a function of temperature, absorption and minority carrier lifetime measurements were performed on samples (Fig.1.b) placed in a LN2-cooled JANIS cryostat showed in Fig.2.b. Figure 2.a and b show the principle used for the absorption measurement. We determined the absorption coefficient through IR transmission measurements using a VERTEX 70v Fourier Transform Infrared (FTIR) spectrometer. The absorption was found from the ratio of the transmissions measured by the FTIR Spectrometer for two samples, the first one is the substrate only and the second one is the dedicated sample (Fig.1.b) with the same substrate. The absorption coefficient is then deduced using $\alpha(\lambda) = -ln(1 - A(\lambda))/d$ with A the absorption and d the thickness of the InAs/InAsSb T2SL region.

For the device properties, the single pixel detectors (Fig.1.a) were wire bonded onto a pin LCC and placed in the cryostat with a ZnSe window (Fig.2.d). The quantum efficiency (QE) is measured using a blackbody source cavity CI Systems SR-200 with temperatures ranging from 973K to 1273K and a narrow bandpass filter [$3\mu m$;

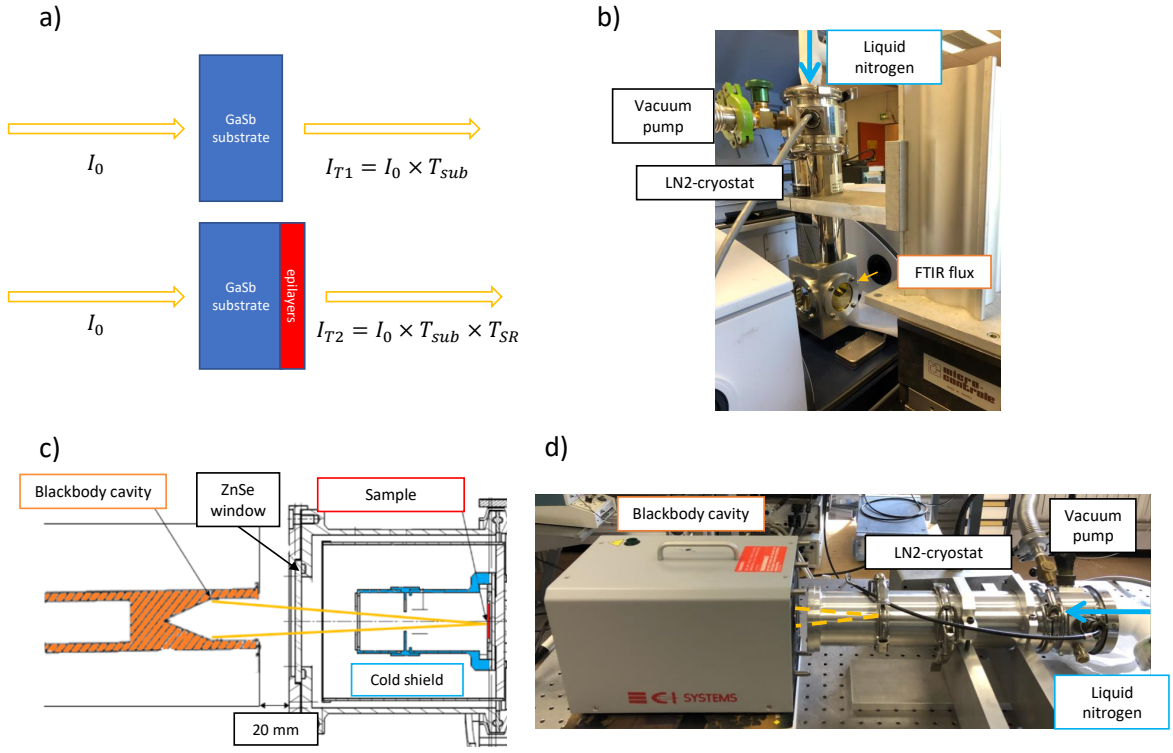

Figure 2: a) Principle of the FTIR transmission measurement in order to get the absorption of the SL absorber layer. b) Photo of the bench used for FTIR transmission measurement. c) Schematic of the illumination of the sample (Fig.1.a) with the blackbody cavity. d) Photo of the experimental bench for quantum efficiency measurement, consisting of the cryostat facing the blackbody cavity.

$3.5\mu m$]. These measurements were performed in front-side illumination configuration, in which light enters the device through the CL and then the photons not absorbed by the AL are completely absorbed by the substrate. In this configuration, the quantum efficiency is single-pass only. Spectral measurements were performed beforehand using a FTIR Spectrometer. The dark current measurements were realized with the same bench, but without blackbody cavity and by blocking incident flux on the sample.

3. EXPERIMENTAL RESULTS

3.1 Absorption and minority carrier lifetime measurements

Figure 3.a shows the measured absorption coefficient in the temperature range 90K-220K of the InAs/InAsSb absorber region. The absorption was found from the ratio of the transmissions measured by the FTIR Spectrometer for two samples with the same substrate. The coefficient is then deduced using $\alpha(\lambda) = -ln(1 - A(\lambda))/d$. The first sample is the dedicated sample (Fig.1.b). The second sample is the substrate alone with no epilayers deposited on it. At $\lambda = 3.4\mu m$, the absorption coefficient reaches $\alpha = 4800cm^{-1}$ at 150K, which is a good absorption value when compared to reported values of InAs/InAsSb with nearby period's thickness[13–15] and when compared to InAs/GaSb which reaches an approximate value of $3300cm^{-1}$.[16] The temperature study of the absorption shows only a red-shift of the absorption edge associated with a superlattice bandgap decrease with increasing temperature, the overall absolute value is relatively constant.

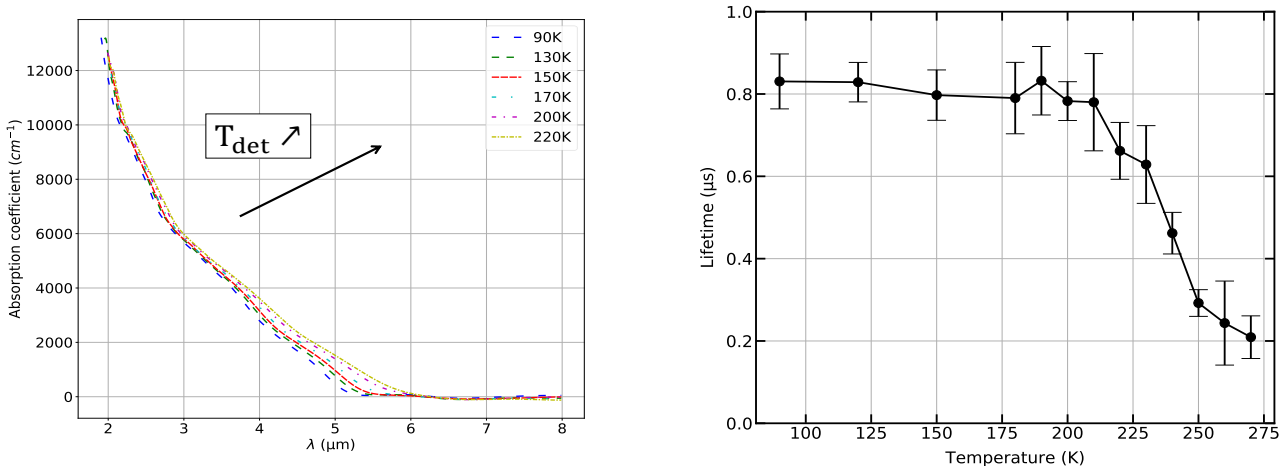

(a) Measured absorption coefficient of the InAs/InAsSb dedicated sample (Fig.1.b) for different temperatures.

(b) Evolution of the measured minority carrier lifetime with temperature. Error bars are plotted to illustrate the measurement precision with the set-up

Figure 3: Results of material properties measurements

Lifetime measurements are realized on structure samples will the full XBn design but that were not etched. The lifetime is studied with temperatures (see Fig.3.b) through time resolved photoluminescence technique.[17–19] We can observe that the lifetime remains constant in the temperature range 90K-200K with an approximate value of 850 ns and then starts dropping. This temperature independence indicates that minority carrier lifetime is limited by SRH processes as reported in,[20] in which a similar result was obtained. Improvement in material quality is required to increase the absolute lifetime value.

3.2 Dark current and photoresponse measurements

A Keithley 6430 sourcemeter is used to apply bias and measure the current delivered by the photodetectors. Figure 4.a shows the measured dark current density as a function of applied bias for temperatures ranging from 90K to 325K. Under 170K, the shapes of the J-V curves show that the dark current is no longer in the diffusion limited regime. Figure 4.b shows an Arrhenius plot of the temperature dependence of dark current density under -0.4V bias. A fit over the temperature range 170K-250K to the expression Aexp(-E_a/k_BT) yields an activation energy of $E_a = 290meV$ which is close to the bandgap (250 meV at 150K). This slight difference can be explained by the presence of a hole-blocking energy barrier between the absorber layer and the barrier layer, which is discussed below. In the temperature range 110K-150K, the GR regime is identified which indicates that a depletion region is formed at the absorber-barrier interface and extends into the absorber, since it is the less targeted doped region between the two.[12] The -0.4V dark current density at 150K is $4.5 \times 10^5 A/cm^2$ which is approximately 10 times the Rule07.[21]

Figure 5 shows the experimental QE of the device in temperature range [90K-220K] and under two applied biases $V = -0.2V$ & $-0.4V$. The detector cutoff wavelength is 5 µm at 150K which is in good agreement with the targeted cutoff wavelength with this design. We can observe that the QE is not fully reached at low temperatures for $V = -0.2V$, which is probably due to the presence of a valence band offset. At $V = -0.4V$, the barrier seems to be overcome, the QE increases in temperature and saturates at 200K. That is why, measurements with bias voltage are performed at different temperatures and presented in Fig.6. High values of QE are obtained compared to the maximum external quantum efficiency that can be reached which is around 55% since no AR coating was applied. Knowing the good absorption properties measured, it is also a sign of good transport properties. The QE increases with applied bias until a certain value is reached and then it starts to "saturate". The behaviour confirms the presence of an unintended barrier in the valence band or valence band offset (VBO). Indeed, as the bias increases the VBO decreases and minority carrier holes can pass the VBO to reach the CL. The VBO is relatively large since the bias, called optimal bias V_{op}, at which saturation occurs is important($V_{op} = -0.3V$ at 150K for example), which means an important bias has to be applied to completely remove the VBO. Moreover,

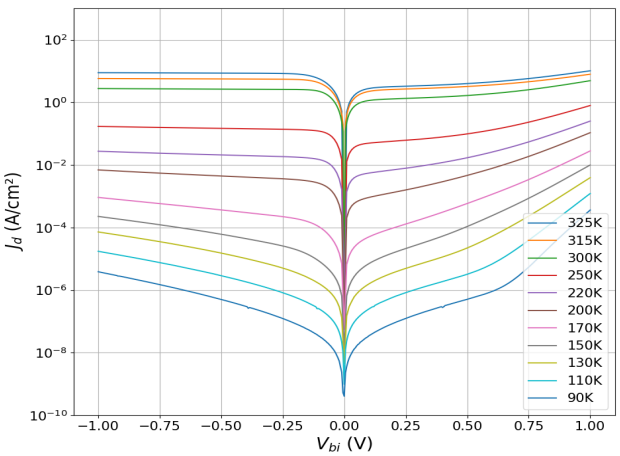

(a) Dark current density (J_d) as a function of applied bias V, measured at temperatures ranging from 90K to 325K.

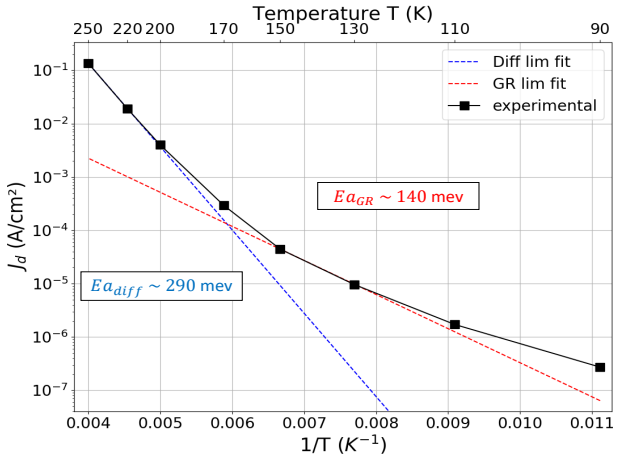

(b) Arrhenius plot of the dark current density. Diffusion and Generation-Recombination regimes are identified.

Figure 4: Temperature dependence of the dark current density (J_d) at V = -0.4V.

a peculiar feature is observed : the QE at 0V which is at 0% for low temperatures increases to reach non negligible values (8% at 220K) as the detector's temperature is increased. The thermal energy is not sufficient to help carriers pass the VBO, we suspect a band bending from the depletion region's evolution with temperature. Further investigation is needed to understand this observation.

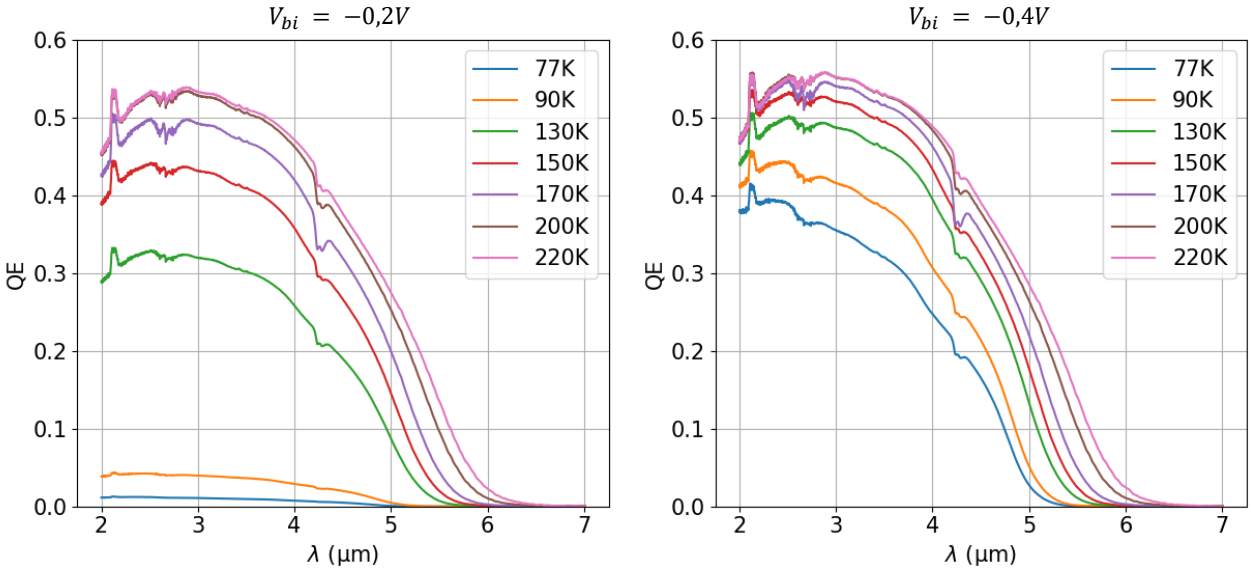

Figure 5: Evolution of the QE with the temperatures range 77K-220K at fixed voltage. QE is for a frontside illuminated photodetector without antireflection coating.

It can be observed that at low temperatures, the QE does not saturate with bias voltage while it is the case at 200K. In order to properly observe this phenomenon, we select the value of QE at $\lambda = 3.4\mu m$ and plot them as a function of applied bias in Fig.6 in the temperature range 77K-220K.

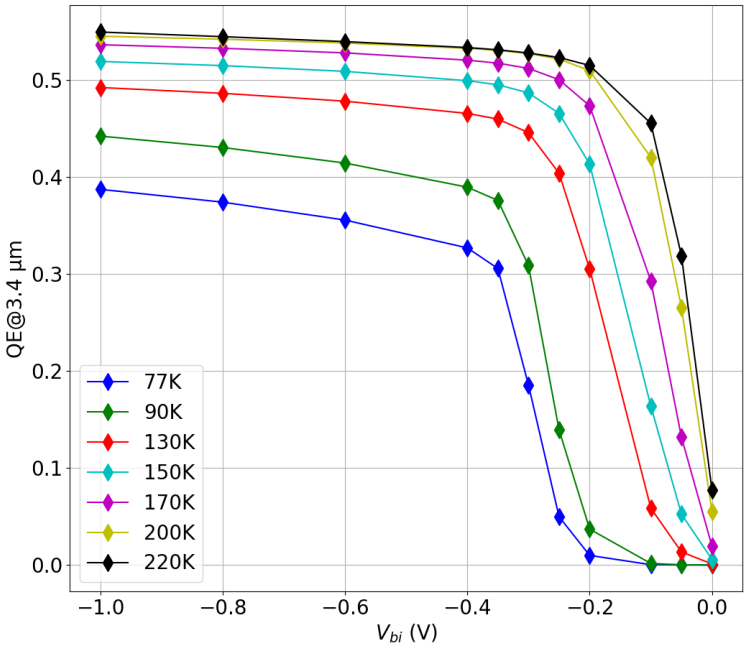

Figure 6: Evolution of the QE at 3.4 μm with the bias voltage in the temperature range 77K-220K. QE is for a frontside illuminated photodetector without antireflection coating.

The QE increases from 32% at T = 77K and $V_{op} = -0.4V$ to reach 54% at T = 200K-220K and $V_{op} = -0.3V$. This evolution with temperature is essentially from an increase of the hole minority carrier diffusion length, since absorption measurements showed no significant evolution of the absorption coefficient with temperatures (Fig.3). The QE increase with bias after V_{op} has been reached is due to the increase of the depletion region width in the absorber. The optimal biases are high compared to other reported values.[13,22] However, the optimal bias can be reduced by adjustments in the AlAsSb composition or doping. At low temperatures the slope of the QE is important after the optimal bias is reached. It means that the diffusion length achieved is not enough and the depletion region helps to collect the minority carriers. Indeed, in the XBn barrier device, photons are absorbed in the absorber region, where electron-hole pairs are generated. Then hole minority carriers should have a sufficient diffusion length compared to the absorber region's length to be able to get past the barrier and be collected by the CL. If the absorber region's length is longer than the diffusion length, some of the photoexcited carriers recombine before reaching the contacts. However, if a depletion region is present, photoexcited carriers are swept into the contact by the electrical field, which increases the QE.

4. DISCUSSION

In order to extract the diffusion length achieved by the photodetector and confirm our analysis, we decided to simulate the QE of this design with a fully analytic model, using Hovel's expressions.[11] Some assumptions for the calculation have been made which include : Low-level injection, uniform material : spatially invariant parameters, zero excess minority carriers at the depletion edge, uniform absorption coefficient, negligible recombination in the depletion region and negligible majority carrier current. The continuity equation of the current density can then be solved, and the analytical solution for quantum efficiency in the different regions of the bariode can be obtained by using a set of boundary conditions. Figure 7 shows the cross-section of the photodiode used in this model. The n-region consists of the neutral region in the AL, the depletion region is formed in the AL and the p-region is neglected since it forms inside the BL which has very high bandgap compared to AL's bandgap.

Light is incident on the CL layer side (front-side illumination) of the bariode, the continuity equation for the minority holes of the n-type material is :

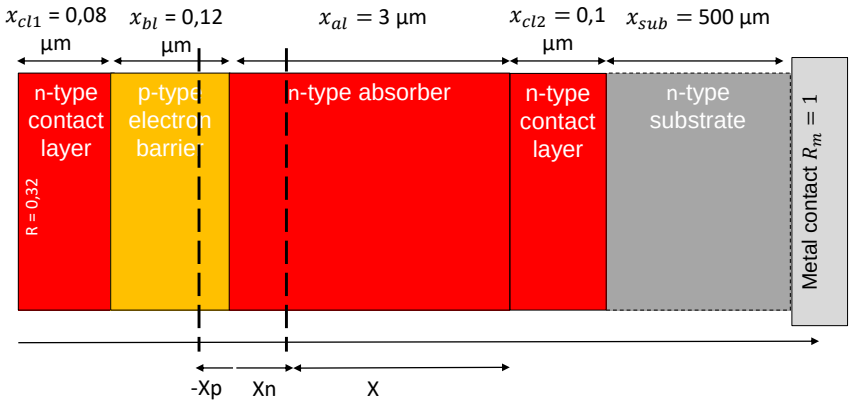

Figure 7: Schematic of the device cross-section for XBn diode. The depletion region is materialized with the region between the dashed lines.

$$D_p \frac{\partial^2(\Delta p)}{\partial x^2} + \mu_p E \frac{\partial(\Delta p)}{\partial x} - G_p + \frac{\Delta p}{\tau_p} = 0 \tag{1}$$

where D_p is the hole diffusion coefficient, μ_p is the hole mobility, E the external electric field, G_p is the optical generation rate, and τ_p the hole recombination lifetime.

The optical generation rate is given by :

$$-G_p(\lambda) = \alpha(\lambda) F(\lambda)(1 - R(\lambda)) \exp(-\alpha(\lambda)x) \tag{2}$$

where α is the absorption coefficient, F is the total number of incident photons per unit area per second per unit bandwidth, and R the reflectivity of the air/T2SL interface (no antireflection coating).

Under steady-state conditions, with zero external electric field, Eq. (1) can be solved using two boundary conditions : at the junction edge, there is no accumulation of carriers since they are drifted by the electric field inside the depletion region $\Delta p[x = x_{cl1} + x_{bl} + x_n] = 0$; on the other side, we consider that no surface recombination takes place $\Delta p[x = x_{cl1} + x_{bl} + x_n + X] = 0$, this assumption does not change the shape of the curve. The total QE in the device can be written :

$$QE = \frac{1}{qF}(J_n + J_{dr}) = QE_n + QE_{dr} \tag{3}$$

$$QE_{dr} = (1 - R) \times [\exp(-\alpha x_{cl1}) - \exp(\alpha(x_{cl1} + x_n))] \tag{4}$$

$$QE_n = \frac{(1 - R)\alpha L_p}{(\alpha L_p)^2 - 1} \times \exp(-\alpha(x_{cl1} + x_n)) \times \left[\alpha L_p - \frac{\alpha L_p \exp(-\alpha X) + sinh(X/L_p)}{cosh(X/L_p)}\right] \tag{5}$$

with L_p the minority carrier hole diffusion length, x_{cl1}, x_{bl}, x_{al}, x_{sub} are the thicknesses of the contact layer, barrier layer, absorber layer and substrate respectively, X is the thickness of the neutral region in the absorber layer. The Hovel calculated QE is compared to experimental ones at three different temperatures (90 K, 150 K, 200 K) and their corresponding V_{op} in Fig.8. A very good agreement is found, which shows the accuracy of the selected model.

The hole diffusion length L_p is linked to hole mobility μ_p and lifetime τ_p through the relationship :

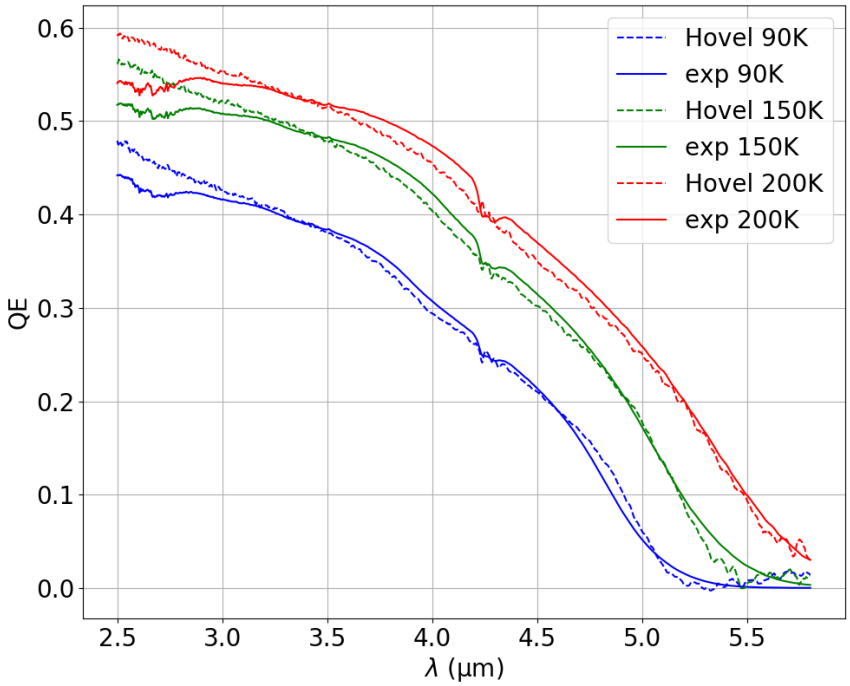

Figure 8: Comparison of experimental QE and the Hovel calculated QE presented in this paper for three temperature : 90 K, 150 K, 200 K, and their respective optimal bias V_{op} : -0.4 V, -0.3 V and -0.25 V

$$L_p = \sqrt{\frac{k_B T}{q} \mu_p \tau_p} \tag{6}$$

From Eq.6 we can then deduce the mobility value. Table 1 gives a summary of the values of the transport properties extracted. As it can be observed at 90K, the diffusion length is inferior to the AL thickness, which confirms the important slope of the QE versus the bias in Fig.6 at low temperature, due to the depletion region extending into the AL. At higher temperatures like 150K, 200K, the diffusion length is superior to the AL thickness, minoirty hole carriers can be collected efficiently. As for the mobility, the values are very small, but they are at state-of-the art values.[9,13] Such low values are reached by the mobility because the hole transport is not through miniband conduction but trap-assisted transport and inter-well hopping transport.[8]

Table 1: Summary of different extracted transport properties from the analytical QE model.

Temperature [K]	Diffusion Length[1]$[\mu m]$	Mobility[2]$[cm^2.V^{-1}.s^{-1}]$	Lifetime[3][ns]
90	1.55	3.64	850
150	3.64	12.1	850
200	7.44	37.7	850

[1] Diffusion length was extracted from the fit of Hovel equations with experimental QE.
[2] Mobility was calculated from the experimental values of lifetime and diffusion length.
[3] Lifetime was obtained via time-resolved photoluminescence (TRPL) measurement.

5. CONCLUSION

In summary, we report the performance of a T2SL detector based on InAs/InAsSb T2SL XBn bariode through experimental measurements and modeling. The quantum efficiency model, based on Hovel expressions was

presented. We measured the material properties absorption and lifetime and used its results to fit the model to the experimental quantum efficiency data. It allowed us to extract the diffusion length of the minority hole carriers in the absorber layer. We found that the diffusion length is shorter than the absorber layer thickness at low temperatures and comparable or longer for temperatures higher than 150K. We then extracted the mobility values, which are very low due to the transport mechanism not being miniband conduction but inter-well hopping transport.

ACKNOWLEDGMENTS

This work was partially supported by the French DGA and by the French National Research Agency (ANR) in the framework of the project HOTMWIR [Contract number N° ANR-18-CE24-0019-02].

REFERENCES

[1] Olson, B., Shaner, E., Kim, J., Klem, J., Hawkins, S., Murray, L., Prineas, J., Flatté, M., and Boggess, T., "Time-resolved optical measurements of minority carrier recombination in a mid-wave infrared inassb alloy and inas/inassb superlattice," *Applied Physics Letters* **101**(9), 092109 (2012).

[2] Ting, D. Z., Soibel, A., Khoshakhlagh, A., Rafol, S. B., Keo, S. A., Höglund, L., Fisher, A. M., Luong, E. M., and Gunapala, S. D., "Mid-wavelength high operating temperature barrier infrared detector and focal plane array," *Appl. Phys. Lett.* **113**(2), 021101 (2018).

[3] Soibel, A., Ting, D. Z., Rafol, S. B., Fisher, A. M., Keo, S. A., Khoshakhlagh, A., and Gunapala, S. D., "Mid-wavelength infrared inassb/inas nbn detectors and fpas with very low dark current density," *Appl. Phys. Lett.* **114**(16), 161103 (2019).

[4] Ariyawansa, G., Duran, J., Reyner, C., and Scheihing, J., "Inas/inassb strained-layer superlattice mid-wavelength infrared detector for high-temperature operation," *Micromachines* **10**(12), 806 (2019).

[5] Wu, D., Li, J., Dehzangi, A., and Razeghi, M., "Mid-wavelength infrared high operating temperature pbn photodetectors based on type-ii inas/inassb superlattice," *AIP Adv.* **10**(2), 025018 (2020).

[6] Deng, G., Chen, D., Yang, S., Yang, C., Yuan, J., Yang, W., and Zhang, Y., "High operating temperature pbn barrier mid-wavelength infrared photodetectors and focal plane array based on inas/inassb strained layer superlattices," *Opt. Express* **28**(12), 17611–17619 (2020).

[7] Zavala-Moran, U., Bouschet, M., Perez, J., Alchaar, R., Bernhardt, S., Ribet-Mohamed, I., de Anda-Salazar, F., and Christol, P., "Structural, optical and electrical characterizations of midwave infrared ga-free type-ii inas/inassb superlattice barrier photodetector," in [*Photonics*], **7**(3), 76, Multidisciplinary Digital Publishing Institute (2020).

[8] Olson, B., Klem, J., Kadlec, E., Kim, J., Goldflam, M., Hawkins, S., Tauke-Pedretti, A., Coon, W., Fortune, T., Shaner, E., et al., "Vertical hole transport and carrier localization in inas/inas 1- x sb x type-ii superlattice heterojunction bipolar transistors," *Phys. Rev. Appl* **7**(2), 024016 (2017).

[9] Casias, L. K., Morath, C. P., Steenbergen, E. H., Umana-Membreno, G. A., Webster, P. T., Logan, J. V., Kim, J. K., Balakrishnan, G., Faraone, L., and Krishna, S., "Vertical carrier transport in strain-balanced inas/inassb type-ii superlattice material," *Appl. Phys. Lett.* **116**(18), 182109 (2020).

[10] Tsai, C.-Y., Zhang, Y., Ju, Z., and Zhang, Y.-H., "Study of vertical hole transport in inas/inassb type-ii superlattices by steady-state and time-resolved photoluminescence spectroscopy," *Appl. Phys. Lett.* **116**(20), 201108 (2020).

[11] Hovel, H. J., "Semiconductors and semimetals. volume 11. solar cells," (1975).

[12] Bouschet, M., Zavala-Moran, U., Arounassalame, V., Alchaar, R., Bataillon, C., Ribet-Mohamed, I., de Anda-Salazar, F., Perez, J.-P., Péré-Laperne, N., and Christol, P., "Influence of pixel etching on electrical and electro-optical performances of a ga-free inas/inassb t2sl barrier photodetector for mid-wave infrared imaging," *Photonics* **8**(6) (2021).

[13] Soibel, A., Ting, D. Z., Fisher, A. M., Khoshakhlagh, A., Pepper, B., and Gunapala, S. D., "Temperature dependence of diffusion length and mobility in mid-wavelength inas/inassb superlattice infrared detectors," *Appl. Phys. Lett.* **117**(23), 231103 (2020).

[14] Rhiger, D. R. and Smith, E. P., "Infrared absorption near the bandgap in the inas/inassb superlattice," in [*Infrared Sensors, Devices, and Applications X*], **11503**, 1150305, International Society for Optics and Photonics (2020).

[15] Webster, P., Riordan, N., Liu, S., Steenbergen, E., Synowicki, R., Zhang, Y.-H., and Johnson, S., "Absorption properties of type-ii inas/inassb superlattices measured by spectroscopic ellipsometry," *Appl. Phys. Lett.* **106**(6), 061907 (2015).

[16] Klipstein, P., Livneh, Y., Glozman, A., Grossman, S., Klin, O., Snapi, N., and Weiss, E., "Modeling inas/gasb and inas/inassb superlattice infrared detectors," *Journal of electronic materials* **43**(8), 2984–2990 (2014).

[17] Donetsky, D., Anikeev, S., Belenky, G., Luryi, S., Wang, C., and Nichols, G., "Reduction of interfacial recombination in gainassb/gasb double heterostructures," *Appl. Phys. Lett.* **81**(25), 4769–4771 (2002).

[18] Connelly, B. C., Metcalfe, G. D., Shen, H., and Wraback, M., "Direct minority carrier lifetime measurements and recombination mechanisms in long-wave infrared type ii superlattices using time-resolved photoluminescence," *Appl. Phys. Lett.* **97**(25), 251117 (2010).

[19] Steenbergen, E., Connelly, B., Metcalfe, G., Shen, H., Wraback, M., Lubyshev, D., Qiu, Y., Fastenau, J., Liu, A., Elhamri, S., et al., "Significantly improved minority carrier lifetime observed in a long-wavelength infrared iii-v type-ii superlattice comprised of inas/inassb," *Appl. Phys. Lett.* **99**(25), 251110 (2011).

[20] Olson, B., Shaner, E., Kim, J., Klem, J., Hawkins, S., Flatté, M., and Boggess, T., "Identification of dominant recombination mechanisms in narrow-bandgap inas/inassb type-ii superlattices and inassb alloys," *Appl. Phys. Lett.* **103**(5), 052106 (2013).

[21] Tennant, W., ""rule 07" revisited: Still a good heuristic predictor of p/n hgcdte photodiode performance?," *J. Electron. Mater.* **39**(7), 1030–1035 (2010).

[22] Rhiger, D. R. and Smith, E. P., "Carrier transport in the valence band of nbn iii–v superlattice infrared detectors," *J. Electron. Mater.* **48**(10), 6053–6062 (2019).